

# New criterion for direct black hole formation in rapidly rotating stellar collapse

Yu-ichirou Sekiguchi and Masaru Shibata

*Graduate School of Arts and Sciences, University of Tokyo, Tokyo, 153-8902, Japan*

## Abstract

We study gravitational collapse of rapidly rotating relativistic polytropes of the adiabatic index  $\Gamma = 1.5$  and 2, in which the spin parameter  $q \equiv J/M^2 > 1$  where  $J$  and  $M$  are total angular momentum and gravitational mass, in full general relativity. First, analyzing initial distributions of the mass and the spin parameter inside stars, we predict the final outcome after the collapse. Then, we perform fully general relativistic simulations on assumption of axial and equatorial symmetries and confirm our predictions. As a result of simulations, we find that in contrast with the previous belief, even for stars with  $q > 1$ , the collapse proceeds to form a seed black hole at central region, and the seed black hole subsequently grows as the ambient fluids accrete onto it. We also find that growth of angular momentum and mass of the seed black hole can be approximately determined from the initial profiles of the density and the specific angular momentum. We define an effective spin parameter at the central region of the stars,  $q_c$ , and propose a new criterion for black hole formation as  $q_c \lesssim 1$ . Plausible reasons for the discrepancy between our and previous results are clarified.

04.25.Dm, 04.30.-w, 04.40.Dg

Typeset using REVTeX

## I. INTRODUCTION

One of the fundamental issues in numerical general relativity is to explore the final fate after gravitational collapse of rotating stellar cores. If their mass is not as large as the maximum mass of a neutron star  $\sim 2M_\odot$ , a rotating neutron star will be the outcome of the collapse. On the other hand, for stars of sufficiently large mass, the collapse will proceed completely and a spacetime singularity will be formed according to the singularity theorems of Hawking and Penrose [1,2]. If the cosmic censorship conjecture suggested by Penrose [3] is correct, any singularity should be surrounded by an event horizon. Then the black hole uniqueness theorems of Israel [4], Carter [5], and Robinson [6] tell that a collapsed star will consequently settle down to a Kerr black hole. On the other hand, if this conjecture is not correct, a rotating stellar collapse might form a state with naked singularities.

It is well known that in a Kerr spacetime, the singularity is covered by an event horizon only if a non-dimensional spin parameter defined as  $q \equiv J/M^2$ , where  $J$  and  $M$  are the angular momentum and the gravitational mass of the system, does not exceed unity [1,2]. Otherwise the singularity is naked. This implies that the value of  $q$  for any black hole cannot be larger than unity. For the realistic progenitor of black holes, however, the value of  $q$  may be larger than unity (see Sec. III A). Thus, it is interesting to explore the final fate after gravitational collapse of rotating stars with  $q > 1$ . Numerical relativity is the unique approach to resolve this problem.

There have been several studies in full general relativity with regard to the above subject on the assumption of axial symmetry [7–13]. A series of simulations of rotating stellar collapse in full general relativity was first performed by Nakamura [7] and his collaborators [8] using the (2+1)+1 formalism developed by Maeda *et al.* [14]. They adopted differentially rotating massive stars that are to collapse (i.e., whose masses are much larger than the maximum allowed mass for a neutron star formation). An interesting finding in their simulations is that  $q$  is an important parameter for determining the prompt black hole formation. Their results suggest that for  $q > 1$ , no black hole is formed and the stars bounce

back due to centrifugal force, indicating that the cosmic censorship conjecture holds. Stark and Piran [9] performed simulations for the collapse of polytropes with the adiabatic index  $\Gamma = 2$  and with an artificially given rigid rotation, using the Bardeen-Piran formalism [15]. They reconfirmed the result found by Nakamura;  $q \sim 1$  is the demarcation between black hole formation and bounce. Abrahams *et al.* [10] studied the collapse of axisymmetric tori consisting of collisionless matter, and also found that black holes form only from initial configurations with  $q \lesssim 1$ . Shibata [11] investigated the effects of rotation and shock heating on the criteria for prompt formation of black holes, for rotating equilibrium polytropes with  $\Gamma = 2$  and  $q < 1$ , and found that effects of rotation and shock heating raise the critical mass for black hole formation. Shibata [12] also studied formation of black holes from marginally stable supramassive rotating neutron stars, modeled by  $\Gamma = 2.5, 2.25, 5/3$ , and  $1.5$  polytropes rotating at the mass shedding limit for which  $q < 1$ , and found that the final state of such collapse is a Kerr black hole with no appreciable disk. Shibata and Shapiro [13] studied the collapse of a rigidly rotating polytrope at the mass-shedding limit with  $\Gamma = 4/3$ . The value of  $q$  for such a configuration is close to unity as  $\approx 0.96$  [16]. They indicate that the final state is a black hole surrounded by an appreciable disk ( $M_{\text{disk}}/M \approx 0.1$ ). All these results seem to suggest that  $q \approx 1$  is the maximum value for the black hole formation, and the final state after the gravitational collapse of rotating stars with  $q < 1$  is a rotating Kerr black hole with a small disk mass.

However, the rotating stellar collapse in general relativity has been not sufficiently studied for *realistic* stellar cores; e.g., iron stellar cores and pair-unstable oxygen cores for which  $\Gamma \lesssim 4/3$  at the onset of the collapse. Recently, Shibata [17] determined marginally stable and rigidly rotating stars with soft equations of state ( $\Gamma \lesssim 4/3$ ) against gravitational collapse, which are plausible initial conditions for rotating stellar core collapse. He indicates that (i) even for a rigidly rotating star with  $q > 1$ , a central region, in which an approximate *local* value of  $q$  ( $q_c$ ) is smaller than unity, will first collapse to form a black hole, unless  $q$  is not too large ( $q < 2.5$ ), and that (ii) as a result of the collapse for  $q_c < 1$  and  $q \gg 1$ , a massive disk ( $M_{\text{disk}}/M = O(0.1)$ ) will be formed around the final black hole.

In this paper, we examine the validity of the conjectures indicated in [17] by axisymmetric simulations in full general relativity. The essence of the points in [17] is that the density profile for the equilibrium stars with  $\Gamma \lesssim 4/3$  is significantly different from that for stiff equations of state, only for which previous works have paid attention [8,9,11,12]. This fact could modify the criterion of black hole formation from previous studies. As a first step toward a more realistic simulation, in this paper, we focus on extracting a physical essence for the criterion of black hole formation using simple toy models. We perform simulations for rotating stellar collapse with a *moderately* soft equations of state of  $\Gamma = 1.5$  and with a stiff equation of state of  $\Gamma = 2$  and compare the results. From the results of these simulations, we illustrate that the global value of  $q$  is an adequate parameter for predicting the black hole formation only for the stiff equations of state but inadequate for the soft equations of state.

The paper is organized as follows. In Sec. II, we briefly describe our formulation, gauge conditions, and boundary conditions. In Sec. III, we first review plausible initial conditions for black hole formation in which the value of  $q$  can be larger than unity. Then, we describe initial conditions adopted in this paper and predict the final outcomes of the stellar collapse for our initial models following [17]. Sec. IV presents numerical results, emphasizing that the predictions made in Sec. III are correct. Sec. V is devoted to a summary. Throughout this paper, we adopt the geometrical units  $G = c = 1$ , where  $G$  and  $c$  denote the gravitational constant and the speed of light, respectively. We use the Cartesian coordinates  $x^k = (x, y, z)$  as the spatial coordinates, with  $r = \sqrt{x^2 + y^2 + z^2}$ .

## II. SUMMARY OF FORMULATION

We perform fully general relativistic simulations for rotating stellar collapse in axial symmetry using the same formulation as in [18], to which the reader may refer for details and basic equations. The fundamental variables for the hydrodynamics are:

$\rho$ : rest mass density,

$\varepsilon$ : specific internal energy,

$P$ : pressure,

$u^\mu$ : four velocity,

$$v^i = \frac{dx^i}{dt} = \frac{u^i}{u^t}, \quad (1)$$

where subscripts  $i, j, k, \dots$  denote  $x, y$ , and  $z$ , and  $\mu$  the spacetime components. As the variables to be evolved in the numerical simulations, we define a weighted density  $\rho_* = \rho \alpha u^t e^{6\phi}$  and a weighted four-velocity  $\hat{u}_i = h u_i = (1 + \varepsilon + P/\rho) u_i$  where  $h$  denotes a specific enthalpy. From these variables, the total baryon rest mass and angular momentum of system, which are conserved quantities in axisymmetric spacetime, can be defined as

$$M_* = \int d^3x \rho_*, \quad (2)$$

$$J = \int d^3x \rho_* \hat{u}_\varphi. \quad (3)$$

General relativistic hydrodynamic equations are solved using a so-called high-resolution shock-capturing scheme [19,18] on the  $y = 0$  plane with the cylindrical coordinates  $(x, z)$  (in the Cartesian coordinates with  $y = 0$ ).

To model initial conditions we adopt the polytropic equations of state

$$P = K \rho^{1+\frac{1}{n}}, \quad (4)$$

where  $n$  is the polytropic index and  $K$  polytropic constant. Then physical units enter the problem only through the polytropic constant  $K$ , which can be chosen arbitrarily or else completely scaled out of the problem. Thus, in the following we display only the dimensionless quantities which are defined as

$$\bar{M}_* = M_* K^{-n/2}, \quad \bar{M} = M K^{-n/2}, \quad \bar{R} = R K^{-n/2}, \quad \bar{J} = J K^{-n}, \quad \bar{\rho} = \rho K^n, \quad \bar{\Omega} = \Omega K^n, \quad (5)$$

where  $M$ ,  $R$ , and  $\Omega$  denote an ADM mass, a radius, and an angular velocity. Hereafter, we adopt the units of  $K = 1$  so that we omit the bar.

On the other hand, during the time evolution, we use the so-called  $\Gamma$ -law equations of state of the form

$$P = (\Gamma - 1)\rho\epsilon, \quad (6)$$

where the adiabatic index  $\Gamma$  is set as  $1 + 1/n$ . In the absence of shocks, no heat is generated and the collapse proceeds in an adiabatic manner, preserving the polytropic form of the equations of state.

We neglect effects of viscosity and magnetic fields. The timescale of dissipation and angular momentum transport due to these effects are much longer than the dynamical timescale, unless the magnitude of viscosity or magnetic fields is extremely large [20]. Thus neglecting them is an appropriate assumption.

The fundamental variables for geometry are:

$$\begin{aligned} \alpha &: \text{lapse function,} \\ \beta^k &: \text{shift vector,} \\ \gamma_{ij} &: \text{metric in 3D spatial hypersurface,} \\ \gamma &= e^{12\phi} = \det(\gamma_{ij}), \\ \tilde{\gamma}_{ij} &= e^{-4\phi} \gamma_{ij}, \\ K_{ij} &: \text{extrinsic curvature.} \end{aligned} \quad (7)$$

As in the series of our papers, we evolve  $\tilde{\gamma}_{ij}$ ,  $\phi$ ,  $\tilde{A}_{ij} \equiv e^{-4\phi}(K_{ij} - \gamma_{ij}K_k^k)$ , and trace of the extrinsic curvature  $K_k^k$  together with three auxiliary functions  $F_i \equiv \delta^{jk}\partial_j\tilde{\gamma}_{ik}$  with an unconstrained free evolution code as in [21–25,11,18].

The Einstein equations are solved in the Cartesian coordinates. To impose axisymmetric boundary conditions, the Cartoon method is used [26]: Assuming the reflection symmetry with respect to the equatorial plane, simulations are performed using a fixed uniform grid with the grid size  $N \times 3 \times N$  in  $(x, y, z)$  which covers a computational domain as  $0 \leq x \leq L$ ,  $0 \leq z \leq L$ , and  $-\Delta \leq y \leq \Delta$ . Here,  $N$  and  $L$  are constants and  $\Delta = L/N$ . In the Cartoon method, the axisymmetric boundary conditions are imposed at  $y = \pm\Delta$ . Details are described in [18] to which the readers may refer.

As the slicing condition we impose an “approximate” maximal slicing condition in which

$K_k^k \approx 0$  is required [21]. As the spatial gauge, we adopt a dynamical gauge condition [27]. In the present work, the equation for the shift vector is written as

$$\partial_t \beta^k = \tilde{\gamma}^{kl} (F_l + \Delta t \partial_t F_l), \quad (8)$$

where  $\Delta t$  denotes a time step in numerical computation [12]. Note that in this gauge condition,  $\beta^i$  obeys a hyperbolic-type equation for sufficiently small value of  $\Delta t$  because the right-hand side of the evolution equation for  $F_i$  contains a vector Laplacian term [25]. The outstanding merit of this gauge condition is that we can save computational time significantly. It has already been found that stable simulations for rotating stellar collapse and merger of binary neutron stars are feasible in this gauge [24,12].

An outgoing wave boundary condition is imposed for  $h_{ij} (\equiv \tilde{\gamma}_{ij} - \delta_{ij})$ ,  $\tilde{A}_{ij}$ , and  $F_i$  at the outer boundaries of the computational domain. The condition adopted is the same as that described in [25]. On the other hand, for  $\phi$  and  $K_k^k$ , outer boundary conditions are imposed as  $r\phi = \text{const}$  and  $K_k^k = 0$ , respectively.

A black hole may be formed as a result of collapse. We determine the location of it using an apparent horizon finder developed in [28]. As the system approaches a stationary state, the apparent horizon will approach the event horizon. In a dynamical spacetime we compute the apparent horizon mass  $M_{\text{AH}}$  which is defined as [29]

$$M_{\text{AH}} = \sqrt{\frac{A}{16\pi}}, \quad (9)$$

where  $A$  denotes area of an apparent horizon.

During the numerical simulations, conservation of mass and angular momentum and a violation of the Hamiltonian constraint,  $H_{\text{error}}$ , are monitored as code checks. Here  $H_{\text{error}}$  is evaluated with a weighted average by  $\rho_*$  as

$$H_{\text{error}} \equiv \frac{\int \rho_* |V| d^3x}{\int \rho_* d^3x} = \frac{1}{M_*} \int \rho_* |V| d^3x, \quad (10)$$

where  $V$  is defined as

$$V \equiv \frac{\tilde{\Delta}\psi - \frac{1}{8}\psi\tilde{R} + 2\pi\psi^5(\rho h w^2 - P) + \frac{\psi^5}{8}\tilde{A}_{ij}\tilde{A}^{ij} - \frac{\psi^5}{12}(K_k{}^k)^2}{\left|\tilde{\Delta}\psi\right| + \frac{1}{8}\left|\psi\tilde{R}\right| + 2\pi\psi^5(\rho h w^2 - P) + \frac{\psi^5}{8}\tilde{A}_{ij}\tilde{A}^{ij} + \frac{\psi^5}{12}(K_k{}^k)^2}. \quad (11)$$

In Eq. (11),  $\psi \equiv e^{4\phi}$ ,  $w \equiv \alpha u^t$ , and  $\tilde{\Delta}$  and  $\tilde{R}$  are the Laplacian and the Ricci scalar with respect to the conformal metric  $\tilde{\gamma}_{ij}$ . Numerical results for several test calculations, including stability and collapse of spherical and rotating neutron stars, have been described in [18].

### III. INITIAL CONDITIONS AND PREDICTIONS

#### A. Candidates for black hole progenitor

In this subsection we review two realistic candidates for the progenitor of black holes and recall that the value of  $q$  for them may be larger than unity.

The first candidate is a degenerate iron core in excess of the Chandrasekhar mass [30,31]. It is well known that stars whose initial mass are larger than  $\sim 8M_\odot$  evolve to form a core mainly composed of iron group elements. Because of iron being the most stable nuclei and no energy generation by nuclear burning, the core contracts gradually. Accordingly the central temperature,  $T_c$ , and central density,  $\rho_c$ , rise to be  $T_c > 10^9$  K and  $\rho_c > 10^9$  g/cm<sup>3</sup>. Then for the stars of initial mass larger than  $\sim 10M_\odot$ , the photo-dissociation of iron to lighter elements occurs first at such hot and dense environments. The entropy of electrons is reduced, as density increases, by the loss of thermal energy due to the photo-dissociation. As a result, the adiabatic index  $\Gamma$  decreases below  $4/3$  and the core is destabilized [30,31]. If mass of the core is much larger than the maximum neutron star mass, a black hole will be formed after the collapse.

The second candidate is a star of very low metallicity or a member of the so-called first stars. Recent numerical simulations of the collapse of primordial molecular clouds have suggested that the first generation of stars contains many massive members of mass  $M > 100M_\odot$  [32–34]. Such massive stars may evolve to form large oxygen core after the helium burning phase [35]. If the oxygen core is sufficiently massive, it will encounter



electron-positron pair creation. As a result, thermal energy that might have gone into raising the temperature and providing more pressure support is diverted to it, bringing its adiabatic index  $\Gamma$  below  $4/3$  to destabilize the core. Following the pair creation, the oxygen-to-silicon and silicon-to-nickel transformation will supply internal energy to the core, which could force back the collapse to explode. However, if mass of the core is sufficiently large, the contraction proceeds and then nickel-to-alpha phase transition will set in, nullifying all decelerating effect of the nuclear burnings. Eventually the core will completely collapse to form a black hole [35,36].

The gravitational collapse sets in when stability of the progenitors changes and, hence, a marginally stable star against gravitational collapse may be regarded as an initial condition for the collapse [17]. Therefore, for both candidates described above, initial conditions for black hole formation are marginally stable rotating stars with adiabatic constant  $\Gamma < 4/3$ . Note that for a configuration with  $\Gamma < 4/3$ , rotation can stabilize it against gravitational collapse.

Indeed, using polytropic equations of state, a stability criterion against gravitational collapse can be written, including rotational effect and post-Newtonian correction as [30,17]

$$3\Gamma - 4 - 2(3\Gamma - 5)\beta - k(\Gamma)\frac{M}{R} < 0, \quad \text{for instability}, \quad (12)$$

where  $\beta$  is the ratio of rotational kinetic energy,  $T$ , to gravitational potential energy,  $W$ , as

$$\beta \equiv \frac{T}{|W|}. \quad (13)$$

$k$  is a parameter which is  $\approx 6.75$  in the case  $\Gamma = 4/3$  and  $R$  is a radius of spherical polytrope. For the progenitor of black holes described above, the compactness  $M/R$  is larger than  $10^3$  and, hence, the general relativistic correction may be neglected. To analyze the effect of rotation, we restrict our attention to the rigidly rotating case for simplicity in the following. Based on a numerical analysis in Newtonian gravity, the maximum value of  $\beta$  for rigidly rotating stars, which is achieved when the velocity at the equatorial surface is equal to the Keplerian velocity (i.e., at the mass-shedding limit), with polytropic equations of state is approximately written as [17]

$$\beta_{\max} \approx 0.00902 + 0.124 \left( \Gamma - \frac{4}{3} \right). \quad (14)$$

Combining Eqs. (12) and (14), it is found that stability criterion becomes as follows:

$$\Gamma \lesssim 1.328, \text{ for instability.} \quad (15)$$

Therefore, the rotation stabilizes the star with  $1.328 \lesssim \Gamma < 4/3$ . This is a crucial result. In a rapidly and rigidly rotating equilibrium state, the spin parameter is related to the compactness parameter  $M/R$  as

$$q \equiv \frac{J}{M^2} \propto \frac{MR^2\Omega}{M^2} \propto \sqrt{\frac{R}{M}}. \quad (16)$$

On the other hand, the value of  $R/M$  for a marginally stable star becomes larger for the smaller value of  $\Gamma$  [17], accordingly increasing the value of  $q$ . Recall that the value of  $q$  is close to unity for a maximally rotating and marginally stable star with  $\Gamma = 4/3$  [16]. Taking all these into account, it is likely that the value of  $q$  exceeds unity for a rapidly rotating and marginally stable star with  $\Gamma$  between 1.328 and  $4/3$ . Actually, it has been shown that this is the case for marginally stable and rigidly rotating polytropes with  $1.328 \lesssim \Gamma \lesssim 1.332$  [17]. Thus, the value of  $q$  for the rapidly rotating progenitor of black hole formation *in nature* is likely to be larger than unity.

## B. Method of preparing initial conditions

We are most interested in the final fate after gravitational collapse of rotating marginally stable stars with  $1.328 \lesssim \Gamma \lesssim 1.332$  and  $q > 1$ . Such simulation is computationally challenging because the dynamical scale changes by a factor of  $\sim 10^4$  during the collapse and also because it is necessary to take into account a realistic equation of state for getting scientific results. Fortunately, the physics that we want to understand (i.e., criterion for black hole formation) can be extracted even from a simulation with appropriate “toy” models. Here, we adopt simplified initial conditions following Stark and Piran [9]: We first give a marginally stable spherical polytrope, and then, add an angular momentum artificially as

well as reduce the pressure to induce the collapse. We choose two values of  $\Gamma$  as 1.5, with which an insight into the collapse of stars with soft equation of state may be gained, and  $\Gamma = 2$ , the value that Stark and Piran adopted.

In more detail, we prepare initial conditions in the following procedure. First, we give a spherical star, marginally stable against gravitational collapse, using the polytropic equations of state with  $\Gamma = 1.5$  or 2.0. Second, we reduce the pressure by an arbitrarily chosen fraction  $f_P$  of its equilibrium pressure. Third, an angular momentum is artificially added according to

$$u_\varphi = e^{4\phi} \varpi^2 u^t \Omega, \quad \text{and} \quad u^t = \sqrt{\frac{-1}{-\alpha^2 + \Omega^2 e^{4\phi} \varpi^2}}, \quad (17)$$

where  $\alpha$  and  $\phi$  denote the lapse function and the conformal factor of the spherical polytrope, and  $\Omega$  is given by

$$\Omega(\varpi) = \Omega_0 \exp \left[ -\frac{\varpi^2}{2R_0^2} \right]. \quad (18)$$

Here,  $\varpi = \sqrt{x^2 + y^2}$  and  $R_0$  is a parameter which controls the degree of differential rotation. For  $R_0 \rightarrow \infty$ , the rotation approaches the rigid rotation (in the following we refer the case with  $R_0 \rightarrow \infty$  as the rigid rotation case). Forth, the Hamiltonian and momentum constraints are reimposed by solving the constraint equations, and then the time evolution is set out.

In Tables I and II, we list characteristic quantities for our initial conditions with  $\Gamma = 1.5$  and 2.0 in the present work.  $R_S = 6.45$  is a coordinate radius of a marginally stable spherical polytrope with  $\Gamma = 1.5$  in the isotropic coordinates and all the quantities are scaled to be non-dimensional using the relations (5).

### C. Predicting the final outcome

Using the same method as described in [17], we predict the final outcome of the collapse for our initial conditions with  $q > 1$ . We pay particular attention to the black hole formation assuming that (i) the collapse proceeds in an axisymmetric manner, (ii) the viscous angular

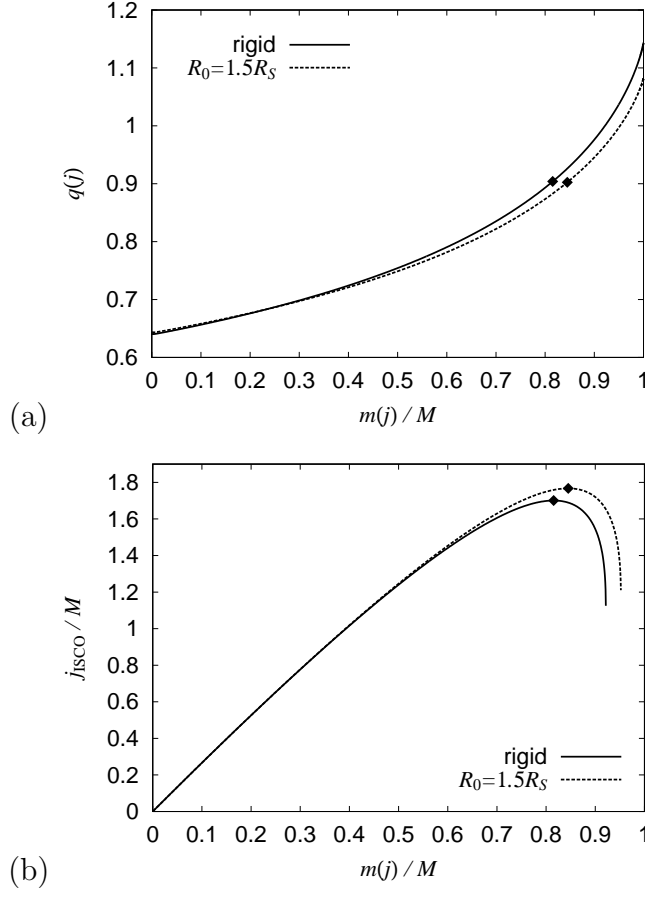


FIG. 1. (a) The distribution of  $q(j)$  and (b)  $j_{\text{ISCO}}$  as a function of  $m(j)/M (= m_*(j)/M_*)$  for models with  $\Omega_0 = 0.065$  and for  $\Gamma = 1.5$ . The solid and dashed curves denote the results for rigid rotation and differential rotation with  $R_0 = 1.5 R_S$ , respectively. The filled diamonds denote values of  $m(j)/M (= m_*(j)/M_*)$  and  $q(j)$  at the maximum value of  $j_{\text{ISCO}}$ .

momentum transport during the collapse is negligible, and (iii) the pressure or heating effects never halt the collapse. Because of the assumption that the viscous effect is negligible during the collapse, the specific angular momentum  $j$  of each fluid element is conserved in an axisymmetric system. Here,  $j$  is defined as

$$j \equiv hu_\varphi. \quad (19)$$

Then we define a rest-mass distribution  $m_*(j)$  as a function of  $j$ , which is the integrated baryon rest mass of fluid elements with the specific angular momentum less than  $j$ :

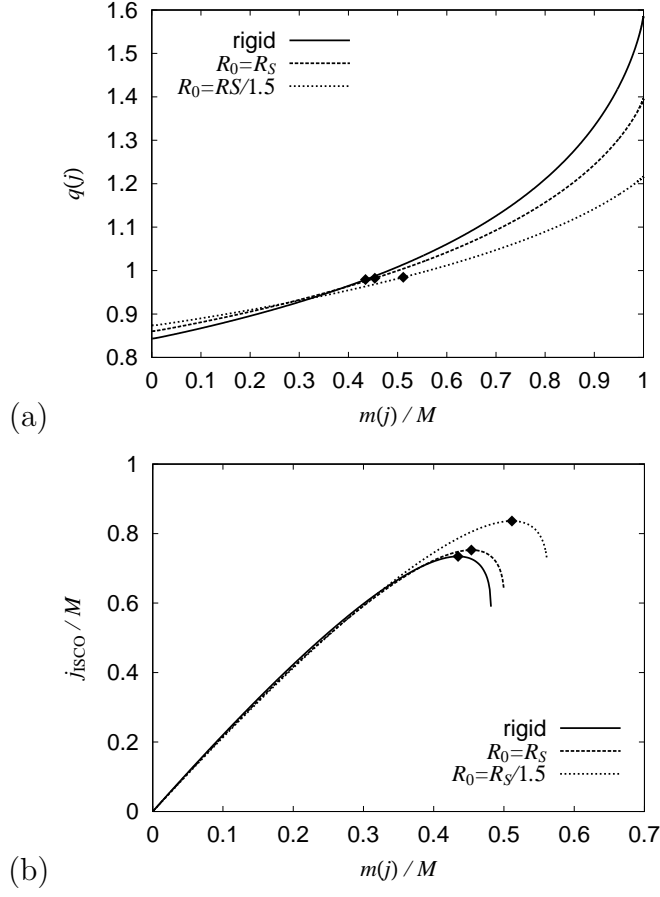


FIG. 2. The same as Fig. 1 but for  $\Omega_0 = 0.090$ . The solid, dashed, and dotted curves denote the results for rigid rotation, differential rotation with  $R_0 = R_S$ , and with  $R_0 = R_S/1.5$ , respectively.

$$m_*(j) \equiv 2\pi \int_{j' < j} \rho_* r^2 dr d(\cos \theta). \quad (20)$$

Similarly, a specific angular momentum distribution is defined according to

$$J(j) \equiv 2\pi \int_{j' < j} \rho_* j' r^2 dr d(\cos \theta). \quad (21)$$

For the following analysis, it is better to have a quasi-local gravitational mass since in contrast with the case of soft equations of state studied in [17], the rest mass and the gravitational mass are different and their difference is not negligible for models adopted in this paper (see Table I). However, the gravitational mass cannot be locally defined in general relativity. Thus, here, assuming the ratio of the quasi-local gravitational mass to the rest mass is uniform inside a star, we define a “gravitational mass distribution” as

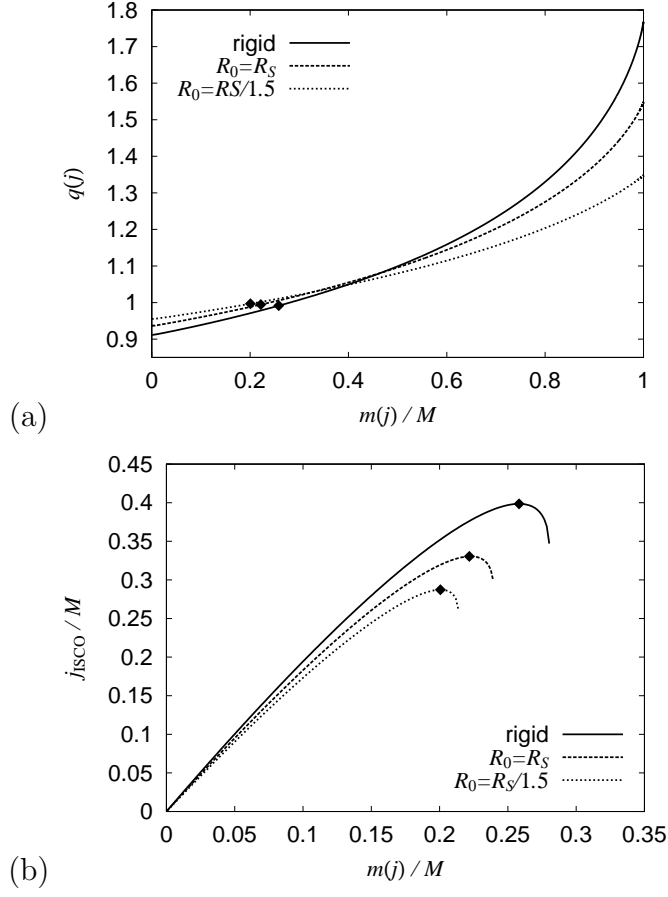


FIG. 3. The same as Fig. 2 but for model of  $\Omega_0 = 0.100$ .

$$m(j) \equiv \frac{M}{M_*} m_*(j). \quad (22)$$

Note that  $m(j)$  is equal to  $M$  for a maximum value of  $j$  (hereafter  $j_{\text{max}}$ ) and that for  $\Gamma \sim 4/3$ ,  $m(j)$  is approximately identical with  $m_*(j)$ .

From these distribution functions, we define spin parameter distributions as

$$q_*(j) \equiv \frac{J(j)}{m_*(j)^2} \quad \text{and} \quad q(j) \equiv \frac{J(j)}{m(j)^2}. \quad (23)$$

These may be approximately regarded as the non-dimensional spin parameters of fluid elements with the specific angular momentum less than  $j$ . Although it is not clear which of two spin parameters is better for the analysis, we adopt  $q(j)$  because of the following reasons: (i) since  $q(j)$  is equal to the global quantity  $q$  for  $j = j_{\text{max}}$ ,  $q(j)$  would be the better quantity

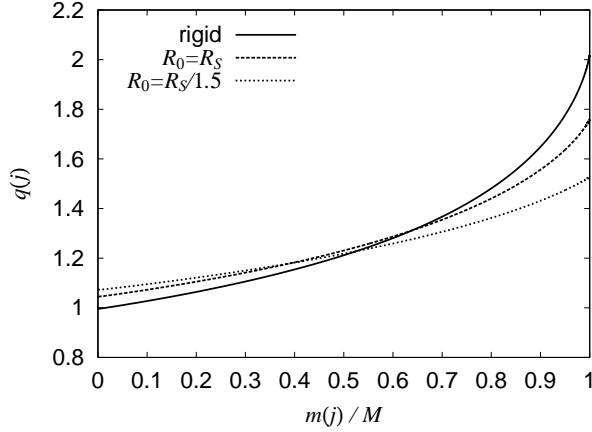


FIG. 4. The same as Fig. 2(a) but for model of  $\Omega_0 = 0.115$ .

for a large value of  $j$ ; (ii)  $M_*$  is always larger than  $M$  for all the models. (This is likely to be the case for all the stable stars.) This implies that  $q(j) > q_*(j)$ . As a result, for  $q(j) < 1$ ,  $q_*(j)$  is always smaller than unity which is the key value for black hole formation.

In Figs. 1(a), 2(a), 3(a), and 4,  $q(j)$  as a function of  $m_*(j)/M_*$  are displayed for the parameters listed in Table I for  $\Gamma = 1.5$ . Figure 5 also shows the same relation for parameters listed in Table II for  $\Gamma = 2.0$ . These figures indicate that the value of  $q(j)$  at the center of stars (hereafter denoted as  $q_c$  and  $q_{*,c}$ ) can be much smaller than unity even if the global values of  $q$  and  $q_*(j_{\max})$  (hereafter denoted simply as  $q_*$ ) are larger than unity. An outstanding difference between the results for two values of  $\Gamma$  is the ratio of  $q/q_c$  for the rigidly rotating case, which is  $\sim 2$  for  $\Gamma = 1.5$  while  $\sim 1.25$  for  $\Gamma = 2$ . This results from the fact that for softer equations of state, the star has a more centrally-condensed structure.

As collapse proceeds, an inner region of the stars collapses faster. This property will be more outstanding for the softer equations of state, with which stars have a more centrally-condensed structure. Taking this and the distribution of  $q(j)$  into account, we conjecture that an inner region of  $q(j) < 1$  may form a seed black hole first and the black hole subsequently grows as the ambient fluids accrete onto it.

Assuming that a seed black hole is formed during the collapse for models of  $q_c < 1$ , we predict the subsequent evolution in the following manner. Here, we focus only on the

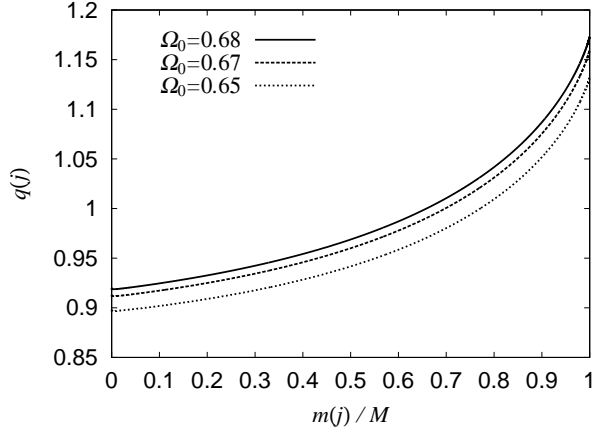


FIG. 5. The same as Fig. 4 but for  $\Gamma = 2.0$ . The solid, dashed, and dotted curves denote the results for  $\Omega_0 = 0.68$ ,  $0.67$ , and  $0.65$  respectively. All the models are rigidly rotating cases.

rapidly rotating case with a large value of  $q > 1$  but with  $q_c < 1$ . Since the centrifugal force of the rapidly rotating progenitors is large, first, the collapse is likely to proceed along the rotational axis to be a disk structure. In such a disk, fluid elements of a cylindrical radius are likely to have the approximately identical value of the specific angular momentum  $j$ . As a result, the fluid elements of the same value of  $j$  will collapse in a simultaneous manner even if they are initially at different locations. Now, let us consider the innermost stable circular orbit (ISCO) around the growing black hole at the center. If the value of  $j$  of a fluid element is smaller than that of the seed black hole at the ISCO,  $j_{\text{ISCO}}$ , the element will fall into the seed black hole eventually. In fact, there is a possibility that some fluids can be captured even for  $j > j_{\text{ISCO}}$  if it is on a noncircular orbit. Ignoring such trajectories yields the minimum amount of fluids that will fall into the black hole. The value of  $j_{\text{ISCO}}$  will change as ambient fluids accrete onto the black hole. If  $j_{\text{ISCO}}$  increases as a result of the accretion, the more ambient fluids will fall into the black hole. This suggests that the evolution of mass  $m_*(j)$  and angular momentum  $J(j)$  inside the seed black hole will approximately proceed according to the initial distribution of  $m_*(j)$  and  $J(j)$  because all viscous effects such as angular momentum transfer are assumed to be negligible. On the other hand, if  $j_{\text{ISCO}}$  decreases during the accretion, no more fluid will fall into the black hole,



and as a result, the dynamical growth of the black hole will terminate.

To estimate the value of  $j_{\text{ISCO}}$  and to predict the growth path of the seed black hole, we assume that the spacetime metric can be instantaneously approximated by that of a Kerr spacetime of mass  $m(j)$  and spin  $q(j)$ . On these approximations, we can compute  $j_{\text{ISCO}}$  of a seed black hole as [30,37,38],

$$j_{\text{ISCO}} = \frac{\sqrt{m(j)r_{\text{ISCO}}} \left( r_{\text{ISCO}}^2 - 2q(j)m(j)\sqrt{m(j)r_{\text{ISCO}}} + (q(j)m(j))^2 \right)}{r_{\text{ISCO}} \left( r_{\text{ISCO}}^2 - 3m(j)r_{\text{ISCO}} + 2q(j)m(j)\sqrt{m(j)r_{\text{ISCO}}} \right)^{1/2}}, \quad (24)$$

where

$$\begin{aligned} r_{\text{ISCO}} &= m(j) \left[ 3 + Z_2 - \{(3 - Z_1)(3 + Z_1 + 2Z_2)\}^{1/2} \right], \\ Z_1 &= 1 + \left[ 1 - q(j)^2 \right]^{1/3} \left[ \{1 + q(j)\}^{1/3} + \{1 - q(j)\}^{1/3} \right], \\ Z_2 &= \left[ 3q(j)^2 + Z_1^2 \right]^{1/2}. \end{aligned}$$

Here,  $m(j)$  and  $q(j)$  are not strictly the gravitational mass and the spin parameter. We suspect that they may have a systematic error of magnitude  $\lesssim |1 - M/M_*|$  for the mass and  $\lesssim 2|1 - M/M_*|$  for the spin parameter. This implies that the estimation of  $j_{\text{ISCO}}$  by Eq. (24) also includes a systematic error. The magnitude of the error for  $j_{\text{ISCO}}$  may be  $\lesssim 10\%$ .

In Figs. 1(b), 2(b), and 3(b), we show  $j_{\text{ISCO}}[m(j), q(j)]$  as a function of  $m_*(j)/M_*$  for  $\Gamma = 1.5$ . These figures show that for models in which the degree of differential rotation is not too high,  $j_{\text{ISCO}}$  has a maximum (hereafter denoted as  $j_{\text{ISCO:max}}$ ). Thus, we predict that the seed black hole will grow until  $j$  reaches  $j_{\text{ISCO:max}}$ . In Table III, we show  $j_{\text{ISCO:max}}$ ,  $m_*(j_{\text{ISCO:max}})$ , and  $q(j_{\text{ISCO:max}})$  for  $\Gamma = 1.5$ . Note that for models of  $\Omega_0 = 0.115$  in which  $q_c > 1$ , we predict that a seed black hole is not formed. Now, let us assume that  $m_*(j_{\text{ISCO:max}})/M_*$  and  $q(j_{\text{ISCO:max}})$  may be approximately regarded as the mass fraction  $M_{\text{BH}}/M$  and spin parameter  $q_{\text{BH}}$  of the final black hole (which is in a quasi-stationary state) as

$$M_{\text{BH}} \approx m(j_{\text{ISCO:max}}), \quad (25)$$

$$q_{\text{BH}} \approx q(j_{\text{ISCO:max}}). \quad (26)$$

From this approximation we immediately predict that an appreciably massive disk ( $M_{\text{disk}}/M = 0.1\text{--}0.8$ ) will be formed after stellar collapse. Note that  $M_{\text{BH}}$  and  $q_{\text{BH}}$  computed above might include a systematic error because of the reason that we approximate a spacetime composed of a black hole and a massive disk simply as a Kerr spacetime. However,  $j_{\text{ISCO}}$  is likely to be determined from the local quantities near the black hole and, hence, we consider that our treatment may be approximately correct.

It should be addressed that for a fixed value of  $q_c$ , the corresponding value of  $q(j_{\text{ISCO:max}})$  is almost independent of the differential rotation parameter  $R_0$ , i.e., the value of  $q$ . This suggests that the spin parameter of the final state of a black hole may be determined by the value of  $q_c$  and independent of  $q$  as far as  $q(j)$  is an increasing function of  $j$ .

In summary, we have predicted the following facts in this section: (I) inner region of a star with  $q_c < 1$  will collapse first to form a seed black hole even if the global value  $q$  exceeds unity significantly; (II) the formed seed black hole will grow as the ambient fluids subsequently accrete onto it, (III) evolution of the relation between the rest mass  $m_*(j)$  and angular momentum  $J(j)$  enclosed inside a growing black hole will agree approximately with the initial relation between  $m_*(j)$  and  $J(j)$ ; (IV) whether black hole is formed or not will be determined by the value of  $q_c$  independent of the value of  $q$ ; (V) the final outcome of a dynamical collapse for a star with  $q_c < 1$  is a black hole surrounded by a disk.

These predictions made from the initial conditions are quite reasonable, but to confirm them, it is obviously necessary to perform fully general relativistic simulations. The next section presents the results of numerical simulation and demonstrates that the predictions are correct.

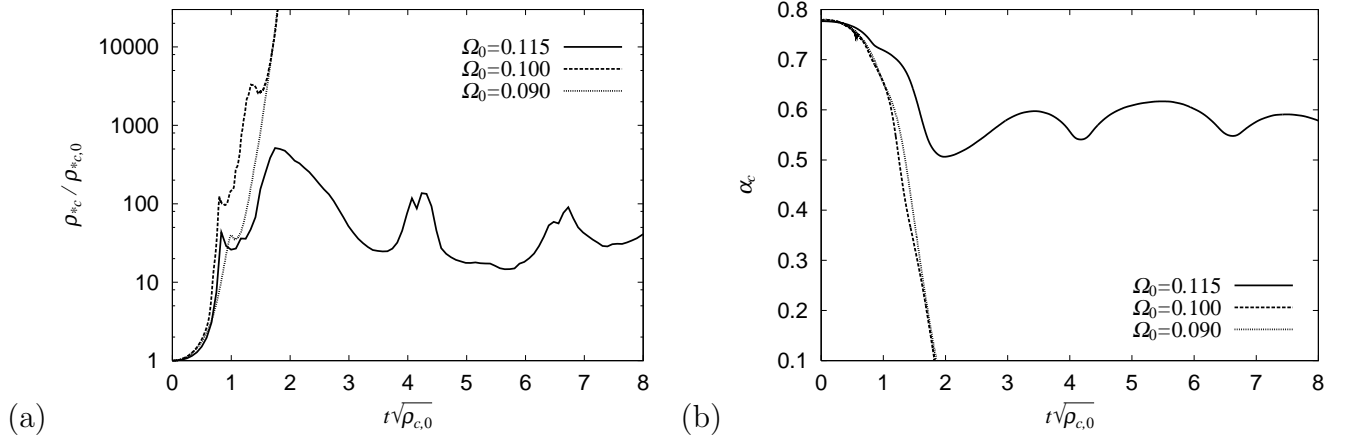


FIG. 6. Evolution of (a) the central density  $\rho_{*,c}$  and (b) the central value of the lapse function  $\alpha_c$  for  $\Gamma = 1.5$ . In both figures, solid, dashed, and dotted curves denote the differentially rotation models of  $R_S = R_0/1.5$  with  $\Omega_0 = 0.090$ ,  $0.100$ , and  $0.115$  ( $q_c = 0.87$ ,  $0.96$ , and  $1.08$ ), respectively.

## IV. RESULTS OF NUMERICAL SIMULATION

### A. Results for $\Gamma = 1.5$

We perform simulations for various initial models with  $\Gamma = 1.5$  listed in Table I, varying grid spacing as  $\Delta x = 0.018$ ,  $0.015$ ,  $0.01125$ ,  $0.009$ , and  $0.006$  (in units of  $G = c = K = 1$ ). In the simulations, the uniform grid is adopted and the outer boundaries along the  $x$  and  $z$ -axes are located at  $L \sim 10$ . Numerical simulation is performed on FACOM VPP5000 in the data processing center of the National Astronomical Observatory of Japan, and personal computers with Pentium 4 processors, each of which has 2 Gbytes memory and a 3.0 GHz clock.

In Fig. 6(a) and 6(b), evolution of the central value of  $\rho_*$  ( $\rho_{*,c}$ ) and the central value of the lapse function  $\alpha_c$  for  $\Gamma = 1.5$  and for the differentially rotation cases with  $R_S = R_0/1.5$  and  $\Omega_0 = 0.090$ ,  $0.100$ , and  $0.115$ . We find that for models with  $q_c < 1$  ( $\Omega_0 \leq 0.100$ ), the collapse proceeds almost monotonically to form an apparent horizon irrespective of values of  $q$  and the differential rotation parameter  $R_0$ . On the other hand, for all the models with  $\Omega_0 = 0.115$  for which  $q_c > 1$ , we find that a black hole is not formed and that the stars

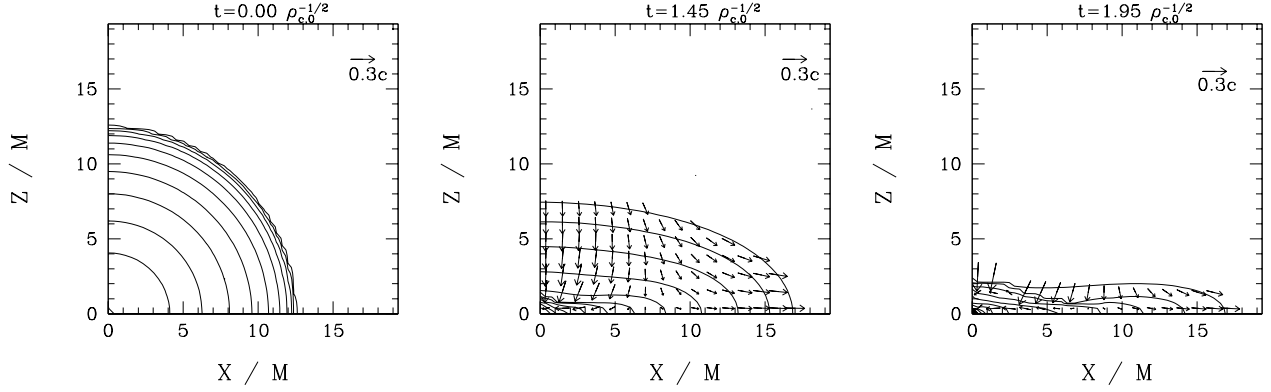


FIG. 7. Snapshots of the density contour curves of  $\rho_*$  and of the velocity field of  $(v^x, v^z)$  at selected time slices for the rigid rotation model with  $\Omega_0 = 0.065$ . The contour curves are drawn for  $\rho_* = \rho_a \times 10^{-0.5j}$ , with  $j = 0, 1, 2, \dots, 10$  where  $\rho_a = 0.011, 1$ , and  $10$  at  $t\rho_{c,0}^{1/2} = 0, 1.45$ , and  $1.95$ . The thick solid circle with the radius  $\sim 0.2M$  of the last panel denotes the apparent horizon.

experience bounces and oscillation. This results from the fact that the centrifugal force near the axis is too strong to form a seed black hole.

In Figs. 7 and 8, we plot snapshots of the density contour curves of  $\rho_*$  and of the velocity field of  $(v^x, v^z)$  at selected time slices for the rigid rotation model with  $\Omega_0 = 0.065$  and for the differential rotation model with  $\Omega = 0.115$  and  $R_0 = R_S/1.5$ . As we predicted in the last section, the collapse first proceeds along the rotational axis ( $z$ -axis) to be a disk-like structure. Then, the disk collapses to the center to form a black hole for  $q_c < 1$ . Irrespective of the models with  $q_c < 1$ , the collapse and the black hole formation proceed in essentially the same manner. For  $q_c > 1$  [see Fig. 8], the centrifugal force is strong enough to prevent a black hole formation. In this case, an oscillating disk is the outcome after the collapse. Such disk may be unstable against a nonaxisymmetric instability.

Even if the value of  $q$  is much larger than unity, a black hole is formed for  $q_c < 1$ , as predicted in Sec. III. To confirm this conclusion strictly, we performed convergence tests varying the grid resolution for a wide range. In Figs. 9(a) and 9(b), we show  $H_{\text{error}}$  and the

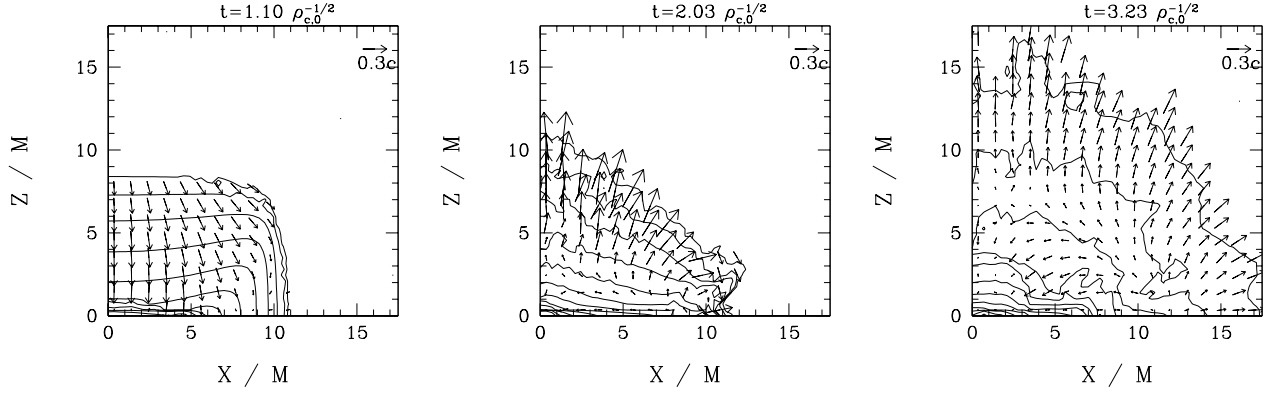


FIG. 8. The same as Figs. 7 but for the differential rotation model with  $\Omega_0 = 0.115$  and  $R_0 = R_S/1.5$ . The contour curves are drawn for  $\rho_* = \rho_a \times 10^{-0.5j}$ , with  $j = 0, 1, 2, \dots, 10$  where  $\rho_a = 1$  for all the time steps.

central density  $\rho_{*,c}$  with different grid spacing ( $\Delta x = 0.009, 0.015$ , and  $0.018$ ) for  $\Omega_0 = 0.065$  and  $R_0 = 1.5R_S$ . These figures illustrate that second-order convergence is achieved.

To accurately determine the threshold values of  $q$  or  $q_c$ , it is also crucial that the rest-mass distribution  $m_*(j)$  as a function of specific angular momentum is conserved accurately at least until the first formation of an apparent horizon. In Fig. 10(a) and 10(b), we compare the rest-mass distribution at  $t = 0$  and at the first formation of apparent horizon for the rigid rotation case with  $\Omega_0 = 0.065$  and  $0.090$ . These figures demonstrate that the rest-mass distribution as a function of  $j$  is conserved well, implying that a spurious numerical transfer of the angular momentum is negligible.

In Fig. 11(a) and 11(b), we show time evolution of the apparent horizon mass for rigid rotation models with  $\Omega_0 = 0.065$  and  $0.090$ . These figures indicate that the process of the black hole formation can be divided into two phases. One is a phase in which a seed black hole is formed at the central region. The other is a phase in which the seed black hole grows as the ambient fluids fall into it. We define the mass of the seed apparent horizon  $M_{\text{AH,seed}}$  from the location of the break of the curves for  $M_{\text{AH}}(t)$ . From this identification, it is found that  $M_{\text{AH,seed}}$  is much smaller than the total mass of the system  $M$  and  $M_{\text{BH}}$  defined in Eq.

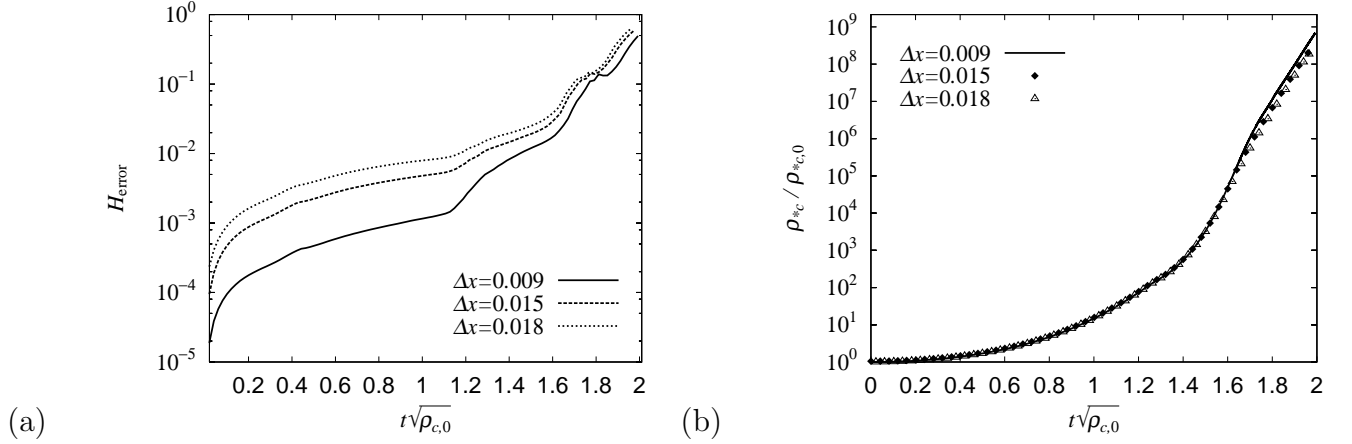


FIG. 9. Time evolution of (a) violation of the Hamiltonian constraint  $H_{\text{error}}$  and (b) the central value of  $\rho_*$  ( $\rho_{*,c}$ ) for  $\Omega_0 = 0.065$  and  $R_0 = 1.5R_S$ . In panel (a), the solid, dashed, and dotted curves denote the results of  $\Delta x = 0.009$ ,  $0.015$ , and  $0.018$ . In panel (b), the filled diamonds and open triangles denote the results of  $\Delta x = 0.015$  and  $0.018$ . These figures indicate that second-order convergence is achieved in our simulations.

(25). As a reasonable result, it is also found that  $M_{\text{AH,seed}}$  is smaller for the larger value of  $\Omega_0$  and  $R_0$  (i.e., for the more rapidly and rigidly rotating cases).

For a Kerr black hole of mass  $M_{\text{BH}}$  and a spin parameter  $q_{\text{BH}}$ , the irreducible mass of the event horizon  $M_{\text{irr}}$  is defined as [2]

$$(M_{\text{irr}}[M_{\text{BH}}, q_{\text{BH}}])^2 \equiv \frac{1}{2}M_{\text{BH}}^2 \left[ 1 + \sqrt{1 - q_{\text{BH}}^2} \right]. \quad (27)$$

If the final state of a black hole can be approximated as a Kerr black hole even though it is surrounded by an appreciable disk,  $M_{\text{AH}}$  should asymptotically approach  $M_{\text{irr}}[M_{\text{BH}}, q_{\text{BH}}]$ . Assuming that  $M_{\text{BH}}$  and  $q_{\text{BH}}$  may be evaluated from the approximate relations (25) and (26),  $M_{\text{irr}}/M$  is  $\approx 0.69$  and  $0.34$  for the rigidly rotating initial data with  $\Omega_0 = 0.065$  and  $0.090$ , respectively (see dotted lines in Fig. 11). We note that for the differentially rotating cases, the value is slightly larger, but it is not significantly different for the same value of  $\Omega_0$ . Thus,  $M_{\text{AH}}$  should approach these values. Actually, the value appears to approach them. Unfortunately, the computations crash in  $\sim 20M$  after the formation of apparent horizons, due to the grid stretching around the black hole horizons, and thus, we cannot confirm this

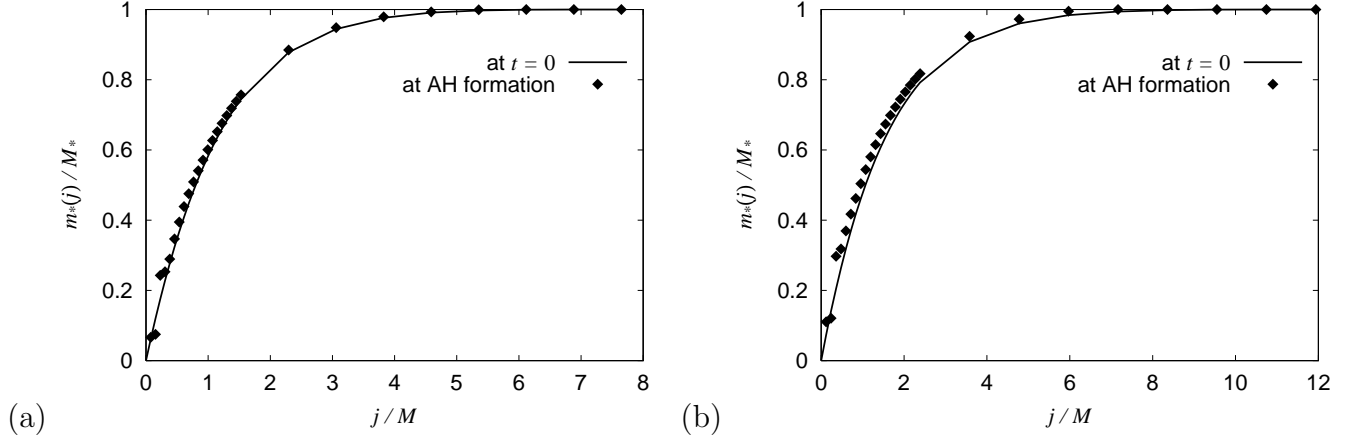


FIG. 10. Rest-mass distribution as a function of specific angular momentum  $j$  (a) for the rigid rotation models with  $\Omega_0 = 0.065$  and (b) for  $\Omega_0 = 0.090$ . In all figures, the solid curves denote the initial rest-mass distributions and the filled diamonds denote the rest-mass distributions when an apparent horizon is first formed. The grid resolution is  $\Delta x = 0.01125$  for (a) and  $\Delta x = 0.006$  for (b).

prediction strictly. To carry out a simulation beyond this time, the so-called black hole excision techniques [39] are necessary.

It should be noticed that  $M_{\text{AH,seed}}$  is always smaller than  $M_{\text{irr}}$  by a factor of  $\sim 2$ . This implies that the black hole significantly grows during the accretion phase. For the realistic progenitor of a black hole formation that have a centrally-condensed density profile, the accretion phase is likely to be much longer than the collapse timescale (defined as  $\rho_{\text{c},0}^{-1/2}$  where  $\rho_{\text{c},0}$  is the central density at  $t = 0$ ). At the accretion phase, the system is composed of a black hole and a surrounding massive disk accreting onto the central black hole. Therefore, this accretion phase might be associated with the gamma ray bursts [40].

For all the models with  $\Omega_0 = 0.100$  in which  $q_c \approx 0.91\text{--}0.96$ , we find that a black hole is formed. However, it is difficult to obtain a convergent result with the present computational setting because of the restriction of the grid resolution. First, recall that the grid spacing required to follow a black hole formation is  $\Delta x \lesssim 0.1M_{\text{seed,AH}}$  (not  $\Delta x \lesssim 0.1M$ ), with which a black hole horizon is covered by  $\sim 10$  grid points. For the model with  $\Omega_0 = 0.100$ , we

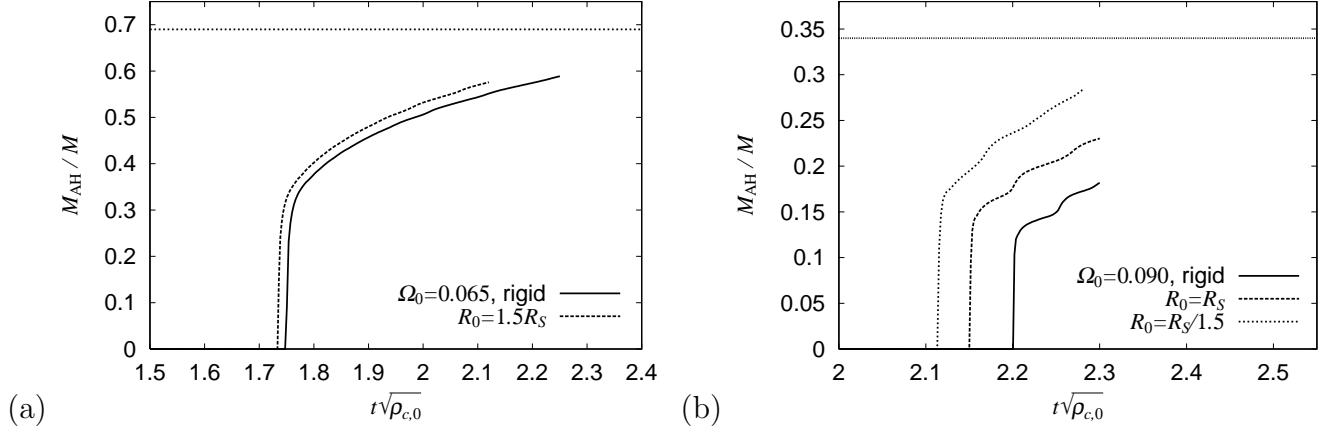


FIG. 11. Evolution of the apparent horizon mass  $M_{\text{AH}}$  for the rigid rotation models with (a)  $\Omega_0 = 0.065$  and (b)  $\Omega_0 = 0.090$ . In both figures the horizontal lines denote the irreducible mass  $M_{\text{irr}}$  with the rigid rotation models,  $\approx 0.67M$  for  $\Omega_0 = 0.065$  and  $\approx 0.34M$  for  $\Omega_0 = 0.090$ .

found that mass of the seed black hole is  $M_{\text{seed,AH}} \lesssim 0.1M$ . This implies that for this model, the required grid spacing is  $\Delta x \lesssim 0.1M_{\text{seed,AH}} \lesssim 0.01M \approx 0.005$ . This value is almost the same as the finest grid spacing we adopt, indicating it difficult to obtain convergent results.

From the above results, we have confirmed the conjectures (I), (II), and (IV) suggested in Sec. III C: We have found that the quasi-local value  $q_c \approx 1$  is an approximate threshold for a seed black hole formation and that after its formation, the black hole grows due to accretion.

To confirm the conjecture (III), we compute the evolution of the total baryon rest mass and the total angular momentum enclosed inside an apparent horizon (denoted as  $m_{*,\text{AH}}(j)$  and  $J_{\text{AH}}(j)$  respectively) at each time step and compare their relation with the initial one between  $m_*(j)$  and  $J(j)$ . In Fig. 12(a), we display evolution of  $m_{*,\text{AH}}(j)$  and  $J_{\text{AH}}(j)$  (the diamonds) together with the initial relation (the solid curve) for the rigid rotation model with  $\Omega_0 = 0.065$ . It is found that an evolutionary track of the black hole is approximately determined by the initial distribution of the mass and the angular momentum, until a numerical error is accumulated significantly. To be more convinced of this result, we also perform an additional simulation for a moderately rotating star (rigid rotation with  $\Omega_0 =$



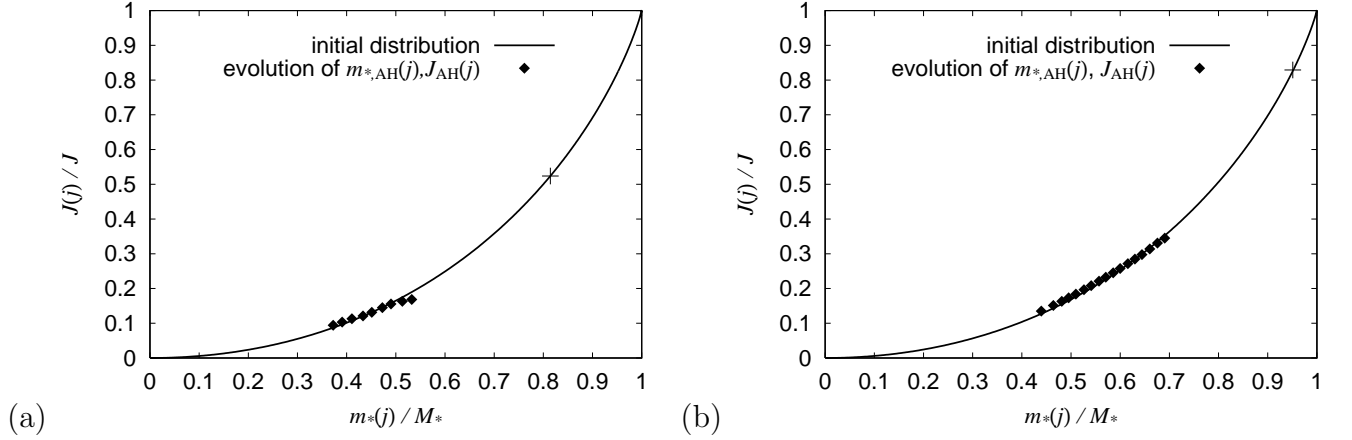


FIG. 12. Evolution of the baryon rest mass  $m_{*,\text{AH}}(j)$  and the angular momentum  $J_{\text{AH}}(j)$  enclosed inside apparent horizons (filled diamonds) for the rigid rotation models with (a)  $\Omega_0 = 0.065$  and (b)  $\Omega_0 = 0.050$ . The solid curve denotes the initial distribution relation of  $m_*(j)$  and  $J(j)$ . The cross denote the location of  $m_*(j_{\text{ISCO: max}})$  and  $J(j_{\text{ISCO: max}})$ , which are the predicted final values of the mass and the angular momentum of a black hole.

0.050). In Fig. 12(b), we show the evolution track of  $m_*(j)$  and  $J(j)$  together with the initial distribution for this case. This figure shows that the initial distribution certainly determines an approximate evolutionary track of the rest mass and the angular momentum enclosed inside the apparent horizon. These results confirm the conjecture (III) of the previous section. This conclusion is quite natural in particular in the present case because we initially deplete the pressure by a significant factor to quickly form a disk-like structure, for which fluid elements of the same value of a cylindrical radius have almost the same value of  $j$ .

To this time, we have confirmed the conjectures (I) – (IV). Now, let us consider the conjecture (V). To confirm it, it is necessary to continue simulations for a long time after formation of apparent horizons. Unfortunately, computations crash in  $\sim 20M$  after the formation of apparent horizons, due to the grid stretching around the black hole horizons. To carry out a simulation beyond this time for confirmation of the conjecture (III), the so-called black hole excision techniques [39] are absolutely necessary.

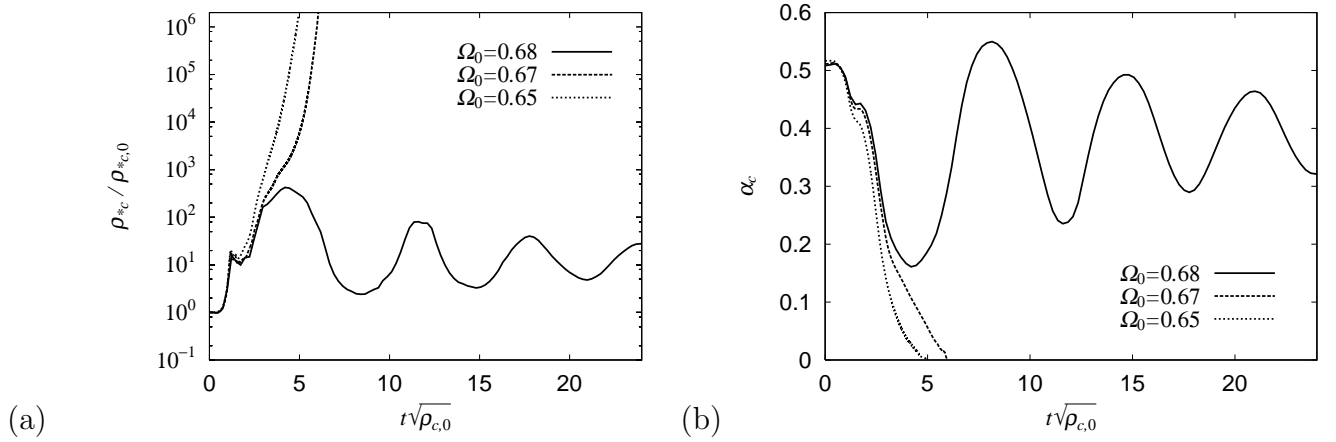


FIG. 13. Evolution of (a) the central density  $\rho_{*c}$  and (b) the central value of the lapse function  $\alpha_c$  for  $\Gamma = 2$ . In both figures, solid, dashed, and dotted curves denote the models of  $\Omega_0 = 0.68$ , 0.67, and 0.65 respectively.

### B. Results for $\Gamma = 2.0$

For comparison with the  $\Gamma = 1.5$  case, we also study rotating collapse adopting a stiff equation of state with  $\Gamma = 2$ . The simulations are performed with  $N = 1000$  and  $\Delta x = 0.005$  (in units of  $G = c = K = 1$ ) for the initial conditions listed in Table II.

From the simulations, we find that a black hole is formed even from the initial data sets with  $q > 1$ . In Figs. 13(a) and 13(b), we show time evolution of the central density  $\rho_{*c}$  and the central value of the lapse function  $\alpha_c$  for models listed in Table II. These figures indicate that the rigidly rotating stars with  $\Omega_0 \lesssim 0.67$  and  $q \lesssim 1.16$  collapse to form a black hole. On the other hand, for rigidly rotating stars with  $\Omega_0 \gtrsim 0.68$  and  $q \gtrsim 1.17$ , a black hole is not formed. Therefore, the threshold value of  $q$  is between these two values. It should be addressed that the present critical value  $q \sim 1.2$  agrees approximately with that found by Stark and Piran [9]. For the critical model, the value of  $q_c$  is  $\approx 0.92$ , close to unity. Since there is no reason to believe that a particularly large value  $q \sim 1.2$  should be the threshold for the black hole formation, we propose the quasi-local value  $q_c \approx 0.92 \sim 1$  as the threshold.

The plausible reason that the critical value of  $q_c$  is somewhat smaller than unity may be

as follows. First note that since configuration of stars with stiffer equations of state is less centrally-condensed and more uniform, the collapse proceeds in a more coherent manner; i.e., the fluid elements collapse to a black hole rather simultaneously. Accordingly, whether a black hole is formed or not after the collapse is likely to be not completely determined by local properties of the stars. Indeed, we find that ratio of the mass of the seed apparent horizon to the total mass of the system for  $\Gamma = 2.0$  is much larger than that for  $\Gamma = 1.5$  case; for  $\Gamma = 2.0$ ,  $M_{\text{AH,seed}}/M \sim 0.35$  at the critical value of  $q_c$ , in contrast with that for  $\Gamma = 1.5$ ,  $M_{\text{AH,seed}}/M \sim 0.1$ . This indicates that for  $\Gamma = 2$ , not  $q_c$  but a value of  $q(j) < 1$  of a moderately large value of  $j$  (denoted as  $j_1$ ) may determine a black hole formation. Since  $q(j)$  is an increasing function of  $m_*(j)$ ,  $1 \sim q(j_1) > q_c$ . Therefore, the threshold value of  $q_c$  may be smaller than unity for stiff equations of state.

Note that for a “realistic” progenitor of black hole formation reviewed in Sec. III A, the associated equations of state are soft ( $\Gamma \lesssim 4/3$ ) ones. Since mass distribution of such stars is significantly centrally-condensed, a demarcation between complete collapse and a bounce will be determined by properties of the central region. Consequently the critical value of  $q_c$  may be almost unity. Furthermore, since the ratio  $M_*/M$  is almost unity for this case,  $q_{*,c} \approx 1$  may be also used as the threshold for black hole formation.

Before closing this section, let us explain the reason that  $q \approx 1$  has been believed as a threshold for black hole formation in the previous works. Stark and Piran used a stiff ( $\Gamma = 2$ ) equation of state [9] as we do. As described above, such stars have rather uniform density distribution and the collapse proceeds in a coherent manner. Furthermore, the distribution of  $q(j)$  expressed as a function of  $m_*(j)$  inside stars with stiff equations of state is rather flat. Indeed, for  $\Gamma = 2.0$  and rigidly rotating case, the ratio of  $q$  to  $q_c$  is  $\sim 1.25$  in contrast with the  $\Gamma = 1.5$  cases for which the ratio is  $\sim 2$  (compare Fig. 5 and Figs. 3(a) for rigid rotation models). These two facts explain the reason that Stark and Piran concluded that  $q \approx 1$  is an approximate threshold for black hole formation.

Nakamura and his collaborators performed simulation for highly differentially rotating stars [7,8]. The higher the degree of differential rotation becomes, the flatter the distribution

of  $q(j)$  is, as indicated in Fig. 4. As a result, the difference between  $q$  and  $q_c$  becomes small for their initial data. This is the reason that the value  $q = 1$  was regarded as the demarcation between black hole formation and a bounce. Abrahams *et al.* [10] performed simulations for toroidal star clusters. Having a toroidal configuration implies that they are highly differentially rotating. Thus, the value of  $q_c$  is likely as large as  $q$ , and hence, the global parameter  $q$  may be used as the threshold.

## V. SUMMARY

We have reported new results about black hole formation in collapse of rapidly rotating stars with  $q > 1$  and with moderately soft ( $\Gamma = 1.5$ ) and stiff ( $\Gamma = 2.0$ ) equations of state, analyzing initial conditions and performing axisymmetric simulations in full general relativity.

The initial conditions are given, following Stark and Piran [9]; we first give marginally stable spherical polytropes with  $\Gamma = 1.5$  or  $\Gamma = 2.0$  and then artificially add an angular momentum. Adopting the same method described in [17], we have predicted that (I) inner region in which  $q_c \lesssim 1$  will collapse first to form a seed black hole even if the global value of  $q$  is much larger than unity; (II) the formed seed black hole will subsequently grow as the ambient fluids accrete onto it; (III) evolution of the relation between the rest mass  $m_*(j)$  and angular momentum  $J(j)$  enclosed inside a growing black hole will agree approximately with the initial relation between  $m_*(j)$  and  $J(j)$ ; (IV) whether black hole is formed or not can be determined by  $q_c$  irrespective of  $q$ ; (V) the final outcome of dynamical collapse will be a black hole surrounded by an appreciable disk.

To confirm these conjectures, we performed fully general relativistic hydrodynamic simulations using a high-resolution shock capturing scheme with the  $\Gamma$ -law equations of state. As a result of numerical simulations, we confirmed the conjectures (I), (II), (III), and (IV). From these results we conclude that the previous criterion for black hole formation that no black hole is formed for  $q \gtrsim 1$  is no longer valid in particular for soft equations of state. As

a new criterion for no black hole formation, we propose the condition  $q_c \gtrsim 1$ .

Associated with conjecture (II), we have found that the process of black hole formation is divided into two phases: the first phase is that a seed black hole is formed and the other is the accretion phase that a part of the ambient fluids are swallowed into the formed seed black hole. At the time of the accretion phase, the system is composed of a black hole and a surrounding massive disk accreting onto the central black hole. In the collapse of massive iron cores, such accretion phase may be associated with the gamma ray bursts [40].

In this paper, we have focused only on the criterion of black hole formation analyzing simple toy models. To obtain a scientific result that can be compared with observational data such as gravitational waves, however, a simulation with a realistic initial condition and a realistic equation of state is necessary. As we indicate in this paper, a rapidly rotating black hole will be formed after rapidly rotating massive stellar core collapse and pair-unstable collapse, if the progenitors are not extremely rapidly rotating at the onset of collapse as  $q_c < 1$ . Formation of a rapidly rotating black hole with  $q \sim 1$  and accretion of a large mass onto such black hole of a large value of  $q$  are likely to be strong burst sources of gravitational waves for laser interferometric detectors. Thus, performing realistic numerical simulations of black hole formation is an important subject for predicting the gravitational waveforms. We plan to attack these computations in a fully general relativistic manner extending previous works [41,42].

For  $q_c > 1$ , a black hole will not be formed promptly. In such case, the collapse leads to formation of a self-gravitating disk or torus. They will be subsequently unstable against nonaxisymmetric deformation. After the nonaxisymmetric instabilities turn on, angular momentum will be transported from the inner region to the outer region, decreasing the value of  $q(j)$  around the inner region below unity. As a result, a seed black hole may be formed. To follow these processes, it is necessary to perform a numerical simulation without assuming the axial symmetry. During the collapse, the typical length scale may change by a factor of  $10^4$  from  $R/M \sim 10^4$  to 1. To follow the collapse by numerical simulation, very large computational resources will be necessary and, thus, the simulation for this phenomenon will

be one of the computational challenges in the field of numerical relativity.

### **Acknowledgments**

Numerical computations were performed on the FACOM VPP5000 machine in the data processing center of National Astronomical Observatory of Japan. This work is in part supported by Japanese Monbu-Kagakusho Grants (Nos. 14047207, 15037204, and 15740142).

## REFERENCES

- [1] S. W. Hawking and G. F. R. Ellis, *The Large Scale Structure of Space-time* (Cambridge University Press, Cambridge, 1973).
- [2] R. M. Wald, *General Relativity* (University of Chicago Press, Chicago, 1984).
- [3] R. Penrose, Riv. Nuovo Cim. **1**, 252 (1969).
- [4] W. Israel, Phys. Rev. **164**, 1776 (1967).
- [5] B. Carter, Phys. Rev. Lett. **26**, 331 (1971).
- [6] D. C. Robinson, Phys. Rev. Lett. **34**, 905 (1975).
- [7] T. Nakamura, Prog. Theor. Phys. **65**, 1876 (1981): **70**, 1144 (1983).
- [8] T. Nakamura, K. Oohara, and Y. Kojima, Prog. Theor. Phys. Suppl. **90**, 1 (1987).
- [9] R. F. Stark and T. Piran, Phys. Rev. Lett. **55**, 891 (1985): T. Piran and R. F. Stark in *Dynamical Spacetimes and Numerical Relativity*, edited by J. M. Centrella (Cambridge University Press, Cambridge, 1986).
- [10] A. M. Abrahams, G. B. Cook, S. L. Shapiro, and S. A. Teukolsky, Phys. Rev. D **49**, 5153 (1994).
- [11] M. Shibata, Prog. Theor. Phys. **104**, 325 (2000).
- [12] M. Shibata, Astrophys. J. **595**, 992 (2003).
- [13] M. Shibata and S. L. Shapiro, Astrophys. J. **572**, L39 (2002).
- [14] K. Maeda, M. Sasaki, T. Nakamura, and S. Miyama, Prog. Theor. Phys. **63**, 719 (1980).
- [15] J. M. Bardeen and T. Piran, Phys. Rep. **96**, 205 (1983).
- [16] T. W. Baumgarte and S. L. Shapiro, Astrophys. J. **526**, 941 (1999).
- [17] M. Shibata, Astrophys. J. **606**, to appear (astro-ph/0403172).

- [18] M. Shibata, Phys. Rev. D **67**, 024033 (2003).
- [19] J. A. Font, Living Review Relativity **6**, 4, 2003: F. Banyuls, J. A. Font, J.-Ma. Ibáñez, J. M. Martí, and J. A. Miralles, Astrophys. J. **476**, 221 (1997).
- [20] T. W. Baumgarte, S. L. Shapiro, and M. Shibata, Astrophys. J. **528**, L29 (2000).
- [21] M. Shibata, Prog. Theor. Phys. **101**, 1199 (1999): Phys. Rev. D **60**, 104052 (1999).
- [22] M. Shibata, T. W. Baumgarte, and S. L. Shapiro, Phys. Rev. D **61**, 044012 (2000): Astrophys. J. **542**, 453 (2000).
- [23] M. Shibata and K. Uryū, Phys. Rev. D **61**, 064001 (2000): Prog. Theor. Phys. **107**, 265 (2002).
- [24] M. Shibata, K. Taniguchi, and K. Uryū, Phys. Rev. D **68**, 084020 (2003).
- [25] M. Shibata and T. Nakamura, Phys. Rev. D **52**, 5428 (1995).
- [26] M. Alcubierre, S. Brandt, B. Brügmann, D. Holz, E. Seidel, R. Takahashi, and J. Thornburg, Int. J. Mod. Phys. D **10**, 273 (2001).
- [27] M. Alcubierre, B. Brügmann, D. Pollney, E. Seidel, and R. Takahashi, Phys. Rev. D **64**, 061501 (2001): L. Lindblom and M. A. Scheel, Phys. Rev. D **67**, 124005 (2003).
- [28] M. Shibata, Phys. Rev. D **55**, 2002 (1997).
- [29] J. W. York, Jr. and T. Piran, in *Spacetime and Geometry: The Alfred Schild Lectures*, edited by R. A. Matzner and L. C. Shepley (University of Texas Press, Texas, 1982).
- [30] S. L. Shapiro and S. A. Teukolsky, *Black Holes, White Dwarfs, and Neutron Stars* (Jon Wiley & Sons, New York, 1983).
- [31] S. E. Woosley, A. Herger, and T. A. Weaver, Rev. Mod. Phys. **74**, 1015 (2002).
- [32] T. Abel, G. Bryan, and M. L. Norman, Astrophys. J. **540**, 39 (2000).



- [33] F. Nakamura and M. Umemura, *Astrophys. J.* **548**, 19 (2001).
- [34] V. Bromm, P. S. Coppi, and R. S. Larson, *Astrophys. J.* **564**, 23 (2002).
- [35] J. R. Bond, W. D. Arnett, and B. J. Carr, *Astrophys. J.* **280**, 825 (1984).
- [36] C. L. Fryer, S. E. Woosley, and A. Heger, *Astrophys. J.* **550**, 372 (2001).
- [37] J. M. Bardeen, W. H. Press, and S. A. Teukolsky, *Astrophys. J.* **178**, 347 (1972).
- [38] V. P. Frolov and I. D. Novikov, *Black Hole Physics* (Kluwer Academic Publishers, Dordrecht, 1998).
- [39] M. Alcubierre and B. Brügmann, *Phys. Rev. D* **63**, 104006 (2001): L. E. Kidder, M. A. Scheel, and S. A. Teukolsky, *Phys. Rev. D* **64**, 064017 (2001): H.-J. Yo, T. W. Baumagarte, and S. L. Shapiro, *Phys. Rev. D* **66**, 084026 (2002): D. Shoemaker, K. S. Smith, U. Sperhake, P. Laguna, E. Schnetter, and D. Fiske, *Class. Quant. Grav.* **20**, 3729 (2003): M. D. Duez, S. L. Shapiro, and H.-J. Yo, gr-qc/0401076.
- [40] S. E. Woosley, *Astrophys. J.* **405**, 273 (1993): B. Paczynski, *Astrophys. J. Lett.* **494**, L45 (1998): A. I. MacFadyen and S. E. Woosley, *Astrophys. J.* **524**, 262 (1999): A. I. MacFadyen, S. E. Woosley, and A. Heger, *Astrophys. J.* **550**, 410 (2001).
- [41] M. Shibata and Y. Sekiguchi, *Phys. Rev. D* **68**, 104020 (2003).
- [42] M. Shibata and Y. Sekiguchi, *Phys. Rev. D*, to be published.

$\rho_c$	$\Omega_0$	$R_0/R_S$	$M$	$M_*$	$J$	$q$	$q_*$	$q_c$	$f_P$
0.005	0.050	$\infty$ (rigid)	0.510	0.530	0.227	0.87	0.81	0.50	0.35
0.005	0.065	$\infty$ (rigid)	0.512	0.535	0.300	1.14	1.05	0.64	0.25
0.005	0.065	1.5	0.501	0.534	0.282	1.08	0.99	0.64	0.25
0.005	0.090	$\infty$ (rigid)	0.529	0.546	0.444	1.59	1.49	0.84	0.1
0.005	0.090	1.0	0.519	0.541	0.377	1.40	1.29	0.86	0.1
0.005	0.090	2/3	0.511	0.537	0.319	1.22	1.11	0.87	0.1
0.005	0.100	$\infty$ (rigid)	0.538	0.552	0.512	1.77	1.68	0.91	0.01
0.005	0.100	1.0	0.524	0.545	0.427	1.55	1.44	0.94	0.01
0.005	0.100	2/3	0.514	0.540	0.358	1.36	1.23	0.96	0.01
0.005	0.115	$\infty$ (rigid)	0.562	0.563	0.640	2.03	2.02	1.01	0.01
0.005	0.115	1.0	0.540	0.553	0.515	1.77	1.68	1.05	0.01
0.005	0.115	2/3	0.526	0.546	0.319	1.54	1.42	1.08	0.01

TABLE I. Central density  $\rho_c$ , angular velocity of rotation axis  $\Omega_0$ , differential rotation parameter  $R_0$  ( $R_S$  is the coordinate radius of the spherical polytrope in the isotropic coordinates), gravitational mass  $M$ , baryon rest mass  $M_*$ , angular momentum  $J$ , the non-dimensional parameter (spin parameter)  $q = J/M^2$ ,  $q_* = J/M_*^2$ , and  $q_c$  of the initial data for models with  $\Gamma = 1.5$  in units of  $G = c = K = 1$ .  $f_P$  denotes a pressure reduction parameter. “rigid” implies the rigid rotation model.

$\rho_c$	$\Omega_0$	$R_0$	$M$	$M_*$	$J$	$q$	$q_*$	$q_c$	$f_P$
0.318	0.65	$\infty$ (rigid)	0.179	0.197	0.0364	1.13	0.93	0.90	0.01
0.318	0.67	$\infty$ (rigid)	0.182	0.199	0.0383	1.16	0.97	0.91	0.01
0.318	0.68	$\infty$ (rigid)	0.183	0.199	0.0393	1.17	0.99	0.92	0.01

TABLE II. The same as I but for models with  $\Gamma = 2.0$ .

$\Omega_0$	$R_0$	$j_{\text{ISCO:max}}/M$	$m_*(j_{\text{ISCO:max}})/M_*$	$q(j_{\text{ISCO:max}})$
0.050	$\infty$ (rigid)	2.29	0.953	0.792
0.065	$\infty$ (rigid)	1.70	0.815	0.904
0.065	$R_S/1.5$	1.77	0.845	0.902
0.090	$\infty$ (rigid)	0.734	0.435	0.979
0.090	$R_S$	0.753	0.454	0.982
0.090	$1.5R_S$	0.836	0.511	0.984
0.100	$\infty$ (rigid)	0.399	0.256	0.992
0.100	$R_S$	0.330	0.222	0.995
0.100	$1.5R_S$	0.287	0.201	0.997

TABLE III. The maximum values of  $j_{\text{ISCO}}$ , and corresponding values of  $m_*(j_{\text{ISCO}})/M_*$  and  $q(j_{\text{ISCO}})$  for  $\Gamma = 1.5$  initial models of  $\Omega_0 = 0.050, 0.065, 0.090$ , and  $0.100$ .